THE JOURNAL OF PHYSICAL CHEMISTRY A

pubs.acs.org/JPCA Article

Probing Orientation-Specific Charge–Dipole Interactions between Hexafluoroisopropanol and Halides: A Joint Photoelectron Spectroscopy and Theoretical Study

Lei Wang, Qinqin Yuan, Wenjin Cao, Jia Han, Xiaoguo Zhou,* Shilin Liu, and Xue-Bin Wang*

Cite This: *J. Phys. Chem. A* 2020, 124, 2036–2045 Read Online

ACCESS | Metrics & More | Article Recommendations | Supporting Information

ABSTRACT: The interactions between hexafluoroisopropanol (HFIP) and halogen anions X^- (F^-, Cl^-, Br^-, and I^-) have been investigated using negative ion photoelectron (NIPE) spectroscopy and ab initio calculations. The measured NIPE spectrum of each $[HFIP{\cdot}X]^-$ (X = Cl, Br, and I) complex shows a pattern identical to the corresponding X^- by shifting to the high electron binding energy side, indicative of the formation of the $[HFIP{\cdots}X^-]$ structure in which X^- interacts with HFIP via charge–dipole interactions. However, the spectrum of $[HFIP{\cdot}F]^-$ appears completely different from that of F^- and is more similar to the spectrum of the deprotonated HFIP anion ($HFIP_{-H}^-$). The geometry and electron density calculations indicate that a neutral HF molecule is formed upon HFIP interacting with F^- via proton transfer, rendering a stable structure of $[HFIP_{-H}{\cdots}HF]^-$. Two conformers of $[HFIP_{-H}{\cdot}HF]^-$ with HFIP being in synperiplanar and antiperiplanar configurations, respectively, are observed, providing direct experimental evidences to show the distinctly different and orientation-specific interactions between HFIP and halide anions.

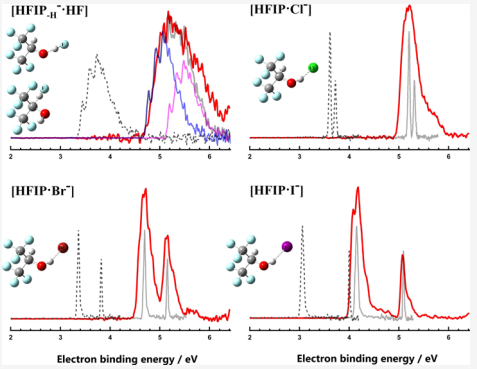

1. INTRODUCTION

Fluorinated alcohols have been extensively used as solvents in various applications in polymer chemistry, organic chemistry, and biological chemistry. As a model fluorinated alcohol, 1,1,1,3,3,3–hexafluoroisopropanol (HFIP, CF_3–C(H)(OH)–CF_3) has attracted wide attention owing to its excellent physicochemical properties. HFIP is miscible with most common polar organic solvents as well as water[1] that makes it an ideal solvent for many polymerization reaction systems.[2−6] It is also widely used in the field of electrochemistry because of its high redox stability.[7,8] In addition, thanks to its small molecular size and potent hydrogen-bonding capacity, HFIP exhibits its importance in many biological systems, for example, as a primary metabolite of the widely used inhalation anesthetic sevoflurane.[9] Moreover, although HFIP is not sensitive to ultraviolet radiation, it is considered to be potential greenhouse gas in the fifth assessment report (AR5) of the Intergovernmental Panel on Climate Change[10] because of its strong absorption in the solar energy range of 8–13 μm, which is well known as the "infrared atmospheric window."[11] Thus, the studies of the related reactions involving HFIP and its derivatives may provide valuable information for solving air pollution and the greenhouse effect.

As a representative multiconformer system, the spectroscopic investigation on the HFIP molecule itself is also very interesting. Single-crystal X-ray analysis of the complex (one piperidine/two HFIP molecules) displayed the existence of three neutral conformers of synclinal (SC), antiperiplanar (AP), and synperiplanar (SP) structures.[12] In the gas phase, the AP conformer was more stable than SC, while the SP conformer was the transition state of two chiral SC structures with a barrier of ~1.0 kJ/mol.[13] Czarnik-Matusewicz et al. measured the mid-infrared spectra of HFIP in carbon tetrachloride and found nearly equal abundances of the SC and AP conformers of the neutral HFIP.[14] To one's surprise, their spectral analysis validated that the AP conformer was more stable than the SC conformer by 0.4 kJ/mol, which was only one-tenth of the previously reported experimental[15] and theoretical[16] energy differences. By analyzing the rotational spectra of HFIP monomers, Shahi and Arunan found that only the AP conformer existed under supersonic expansion conditions.[13] The investigation on the interaction between HFIP and water in the gas phase validated two complex conformers with the structures of $[HFIP(AP){\cdots}H_2O]$ and $[HFIP(SC){\cdots}H_2O]$, of which the former was more stable by about 0.9 kJ/mol, although a stronger binding was found

Received: January 2, 2020
Revised: February 5, 2020
Published: February 20, 2020

https://dx.doi.org/10.1021/acs.jpca.0c00024
J. Phys. Chem. A 2020, 124, 2036–2045

between the SC conformer and H_2O.[17] In solutions, the aggregation of HFIP and water was found to retard rotational motions of water molecules.[18] Similar aggregates were confirmed in the mixed solutions of HFIP, H_2O_2, and the substrate cyclooctene by molecular dynamic simulations.[19]

There are only a few reports about the HFIP and ion interaction,[20−22] although such interaction widely exists in related solutions or ionic liquids. In general, various complex conformers can be formed between HFIP and ions determined by strong charge−dipole interactions. Thus, studying stability of these charged complexes in the gas phase can provide crucial clues for understanding the microstructure of the related salt solutions (or ionic liquids). Here, we chose halides as anions because of their simplicity and as common hydrogen bond (HB) receptors.[23,24] Therefore, the gaseous $[HFIP{\cdot}X]^-$ (X = F, Cl, Br, and I) complexes represent ideal model systems, providing excellent opportunity to spectroscopically characterize their structures and energetics for understanding the charge (halide)−dipole (HFIP) interactions and their effects on conformational stabilization and transformation.

Negative ion photoelectron (NIPE) spectroscopy coupled with electrospray ionization (ESI) has been successfully used to investigate structures and bonding features of many complex anions, for example, *cis*-pinonic acid anion and water,[25] divalent transition metal EDTA complexes,[26] HSO_4^-, and organic acids.[27] The measured difference in electron binding energy (EBE) of the complex anion from the corresponding isolated anion, that is, ΔEBE, can directly reflect the interaction strength between the host neutral molecule and guest anion.[28] In this work, we have generated $[HFIP{\cdot}X]^-$ (X = F, Cl, Br, and I) complex anions and recorded their NIPE spectra. Additionally, density functional theory (DFT) calculations have been performed to obtain the optimized geometries and energies of these complexes in anionic and neutral states. Spectral pattern analyses and quantum calculations identify two classes of molecular binding motifs for $[HFIP{\cdot}X]^-$. In the cases of X = Cl, Br, and I, the complex anions can be regarded as X^- solvated by the neutral HFIP; while for X = F, the cluster is better described as a deprotonated HFIP moiety, that is, $HFIP_{-H^-}$ anion interacted with a neutral HF molecule. The latter structure is facilitated via proton transfer from HFIP to F^- driven by stronger proton affinity (PA) of F^- than $HFIP_{-H^-}$ anion, thus affording the formation of a stable $[HFIP_{-H^-}{\cdots}HF]$ binding configuration.

2. EXPERIMENTAL AND COMPUTATIONAL METHODOLOGIES

2.1. Negative Ion Photoelectron Spectroscopy. The NIPE spectra were measured using the magnetic-bottle time-of-flight (TOF) photoelectron spectrometer at Pacific Northwest National Laboratory, equipped with an ESI source and a temperature-controlled cryogenic ion-trap.[29,30] The complex anions $[HFIP{\cdot}X]^-$ (X = F, Cl, Br, and I) were produced by electrospraying a mixture solution of 1×10^{-3} M HFIP and sodium halide salt using a methanol/water (3/1 ratio) solvent. In order to produce a stronger deprotonated HFIP anion beam, the pH value of the HFIP solution was adjusted to 9−10 by adding 10^{-2} M NaOH aqueous solution dropwise. All anions were transported into vacuum by two radiofrequency-only ion-guides, accumulated, and thermalized at 20 K in the cryogenic 3D trap. The cold anions were then pushed out into the extraction zone of the TOF mass spectrometer at 10 Hz, and the desired anions were each mass-selected and decelerated before being photodetached in the interaction zone with a 193 nm (6.424 eV) laser beam (EX100F, GAM ArF Laser). The laser was operated at a 20 Hz repetition rate with the anion beam off at alternating laser shots, thus enabling shot-by-shot background subtraction. The photodetached electrons were collected with nearly 100% efficiency by the magnetic-bottle and analyzed with a 5.2 m-long electron flight tube. The recorded TOF photoelectron spectrum was converted into an electron kinetic energy spectrum and calibrated with the known transitions of I^- and $Cu(CN)_2^-$. The EBE spectra, presented in the manuscript, were obtained by subtracting the kinetic energy spectra from the detachment photon energy. The electron energy resolution was about 2% (i.e., ∼20 meV for electrons with 1 eV kinetic energy).

2.2. Computational Details. To study the structures, energetics, and spectral features of $[HFIP{\cdot}X]^-$ (X = F, Cl, Br, and I), DFT calculations were performed using the B3LYP, ωB97XD and M06-2X functionals with DFT-D3(BJ) dispersion corrections. The standard 6-311++G(d,p) basis set[31] was used for C, H, O, F, Cl, and Br atoms, and the aug-cc-pVTZ-PP basis set with the Stuttgart−Küln MCDHF RSC ECP (28 core electrons)[32] was employed for the I atom. All these basis sets were obtained from the EMSL Basis Set Exchange.[33] Geometry optimizations of the anions and the corresponding neutrals were carried out without any symmetry constraints. Vibrational frequency analyses were carried out at the same level to ensure that the optimized structures were true minima, and obtained frequencies were used to calculate the zero-point vibrational energies (ZPEs). The theoretical vertical detachment energy (VDE) was calculated as the energy difference between the neutral and the corresponding anion, both at the optimized anion's geometry, while the adiabatic detachment energy (ADE) was computed as the energy difference between the neutral and anion, each at its own optimized geometry.

In the cases of X = Cl, Br, and I, binding energies (BEs) between HFIP and halides X^-, that is $BE(HFIP{\cdot}X^-)$, were determined from the single-point energy calculations according to eq 1, including ZPE corrections and the basis set superposition error (BSSE)[34] corrections using the counterpoise method of Boys and Bernardi[35]

$$BE(HFIP{\cdot}X^-) = E(HFIP) + E(X^-) - E(HFIP{\cdot}X^-) \quad (1)$$

where $E(HFIP)$, $E(X^-)$, and $E(HFIP{\cdot}X^-)$ are the energies of a neutral HFIP moiety, halide anion, and complex anion, respectively, at the optimized structure of the $[HFIP{\cdot}X^-]$ complex. Similarly, in the X = F case, BE was calculated according to

$$BE = E([HFIP_{-H^-}]) + E(HF) - E([HFIP_{-H^-}{\cdot}HF]) \quad (2)$$

with ZPE and BSSE corrections because the complex adopts a $[HFIP_{-H^-}{\cdots}HF]$ binding configuration (vide infra).

Natural bond orbital (NBO) analyses[36] were used to compute natural atomic charges, to compare with the charges derived from the electrostatic potential using the Merz−Kollman−Singh (MK) method,[37] and to provide a valence bond-type description of wavefunction. All these calculations were performed with the Gaussian 09 program package.[38] The electron density topological analysis of each stable configuration was carried out using the theory of "atoms in molecules (AIM)"[39,40] with the Multiwfn program.[41] To analyze the vibrational structure of the EBE spectrum, a Franck−Condon simulation was carried out with the ezSpectrum program.[42] A

https://dx.doi.org/10.1021/acs.jpca.0c00024
J. Phys. Chem. A 2020, 124, 2036−2045

full width at half-maximum (fwhm) of 80 meV was used in the simulated spectra and compared with the experimental spectra.

3. RESULTS AND DISCUSSIONS

3.1. NIPE Spectra of $[HFIP{\cdot}X]^-$ (X = F, Cl, Br, and I).

Figure 1 shows the 193 nm low-temperature NIPE spectra of $[HFIP{\cdot}X]^-$ (X = F, Cl, Br, and I). An extremely broad spectral feature is observed for X = F, spanning EBE from 4.7 to 6.2 eV, while the spectrum becomes much narrower with one band centered at EBE = 5.25 eV for X = Cl. In the cases of X = Br and I, two discrete peaks are resolved. A consistent spectral pattern recognition is readily concluded for the $[HFIP{\cdot}X]^-$ (X = Cl, Br, and I) spectra, that is, the complex anion spectra each being similar to the corresponding isolated X^- but simply shifting to the high EBE side, as shown in Figure 1. The VDE and ADE of $[HFIP{\cdot}I]^-$, determined from the first peak maximum and onset threshold, are 4.15 and 4.03 eV, respectively, where the latter is obtained taking into account the experimental energy resolution (as observed with the blue downward arrow in Figure 1). The energy gap of 0.93 eV for the two bands basically equals to the spin−orbit splitting of iodine (0.943 eV).[43] Similarly, the two dominant peaks are located at EBE = 4.69 and 5.15 eV for $[HFIP{\cdot}Br]^-$ with a 0.46 eV energy gap, nearly identical to the spin−orbit splitting of Br (0.457 eV) ($^2P_{3/2}$ and $^2P_{1/2}$).[43] The VDE and ADE of the Br^- complex are estimated to be 4.69 and 4.52 eV, respectively (Table 1). The spectrum of $[HFIP{\cdot}Cl]^-$ shows one dominant band with VDE = 5.20 eV and ADE = 4.73 eV. A careful examination of the spectrum reveals a shoulder peak at 5.38 eV via double-peak fitting. Such a small gap is consistent with the much reduced spin−orbit splitting of the chlorine atom (0.109 eV).[43]

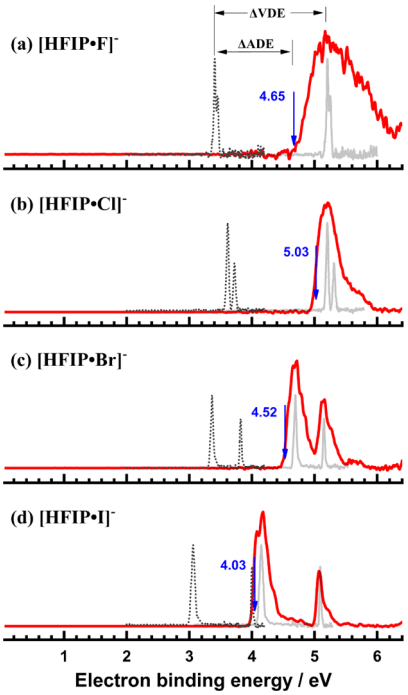

Figure 1. Low-temperature photoelectron spectra of $[HFIP{\cdot}F]^-$, $[HFIP{\cdot}Cl]^-$, $[HFIP{\cdot}Br]^-$, and $[HFIP{\cdot}I]^-$complex anions at 193 nm. The dotted and solid lines in gray show the original and shifted spectra of the free halide anions, which are adapted from ref 44.

Using the experimental EBEs of $[HFIP{\cdot}X]^-$ and X^-, the resulting blueshifts in EBE upon X^- clustering with HFIP, that is, ΔVDE/ΔADE, are obtained to be 1.59/1.42, 1.33/1.16, and 1.09/0.97 eV, for X = Cl, Br, and I, respectively. Evidently, both ΔVDE and ΔADE decrease along X = Cl → Br → I, indicating a gradually reduced interaction strength between the halide and HFIP. Such a BE trend parallels with the PA trend along halide anions (333.5, 324.3, and 315.9 kcal/mol for Cl^-, Br^-, and I^-, respectively).[45] The above spectral analyses clearly imply that the negative charge localizes on the halide moiety in each of these three complexes, which can be regarded as $[HFIP{\cdots}X^-]$ with X^- being the electron emitter. No proton transfer occurs in forming $[HFIP{\cdot}X]^-$ (X = Cl, Br, I) clusters, which is in accordance with the fact that the PA values of these halide anions are all smaller than that of $HFIP_{-H}$, that is, $(CF_3)_2CHO^-$ (338.4 kcal/mol).[46] Moreover, the significantly increased EBEs of these complex anions, as compared to those of free halides, indicate that the negative charge, though still spatially localized on the halide, is greatly stabilized in the complexes, presumably via forming HBs and charge−dipole interactions.

Because the fluorine atom has a very small spin−orbit splitting (~51 meV),[43] only a close-packed doublet exhibits at EBE = 3.4 eV in the F^- spectrum (dotted trace in Figure 1a). If the interactions between F^- and HFIP were similar to the rest of halides, a moderately broadened peak should have been expected. However, the experimental spectrum (Figure 1a) appears completely different from that of F^- and is extremely broad, spanning the EBE range from 4.7 to 6.2 eV with discernible vibrational structures. The ADE of this complex anion is determined to be 4.65 eV, which is ~0.4 eV lower than that of $[HFIP{\cdot}Cl]^-$. The extraordinary breadth of the spectrum implies a completely different molecular structure for $[HFIP{\cdot}F]^-$. Because the PA of F^- (372.7 kcal/mol)[45] is appreciably larger than that of the deprotonated HFIP anion (338.4 kcal/mol),[46] it is reasonable to assume that the complex prefers a

Table 1. Theoretical and Experimental VDEs and ADEs (in eV) for the $[HFIP{\cdot}X]^-$ (X = F, Cl, Br, I) Complex Anions

	VDE				ADE			
species	B3LYP	ωB97XD	M06-2X	expt.	B3LYP	ωB97XD	M06-2X	expt.
$[HFIP{\cdot}F]^-$ (Iso A)	5.31	5.36	5.50	5.51[a]	4.66	4.58	4.91	5.19[a]
$[HFIP{\cdot}F]^-$ (Iso B)	5.08	5.04	5.25	5.08[a]	4.54	4.45	4.81	4.76[a] 4.65[b]
$[HFIP{\cdot}Cl]^-$ (Iso A)	5.21	5.23	5.32	5.20	5.03	5.00	5.00	5.03
$[HFIP{\cdot}Br]^-$ (Iso A)	4.90	4.82	4.85	4.69	4.74	4.64	4.63	4.52
$[HFIP{\cdot}I]^-$ (Iso A)	4.40	4.31	4.18	4.15	4.28	4.18	4.03	4.03
$[HFIP_{-H}]^-$	3.75	3.66	3.57	3.75	3.49	3.39	3.50	3.43

[a]Experimentally estimated ADEs and VDEs via fitting the $[HFIP{\cdot}F]^-$ spectrum (see Section 3.4 for details). [b]The ADE was directly determined from the spectral onset (Figure 1a).

https://dx.doi.org/10.1021/acs.jpca.0c00024
J. Phys. Chem. A 2020, 124, 2036−2045

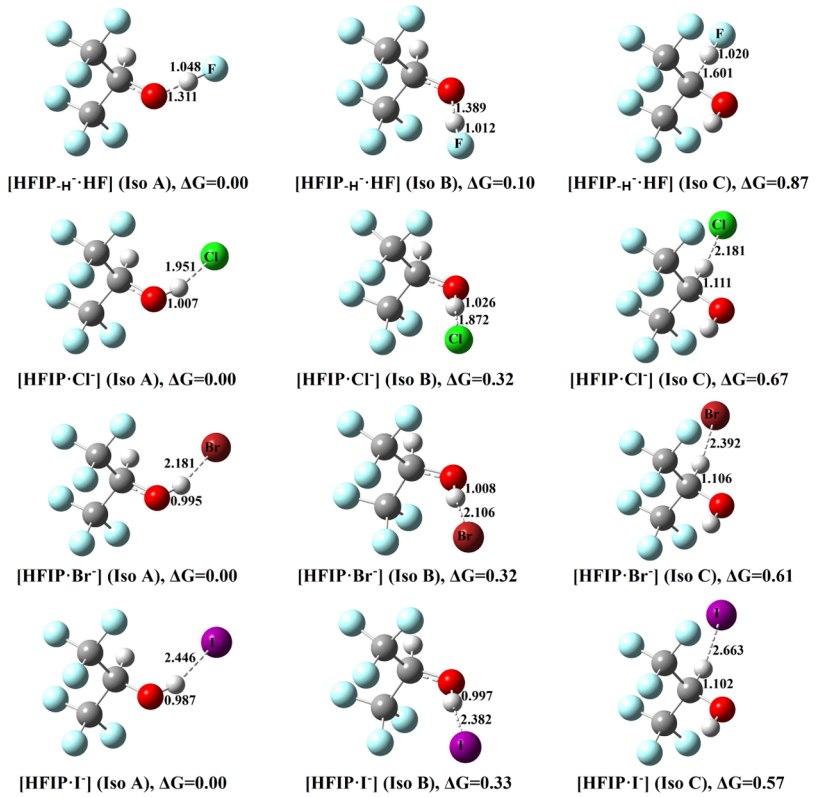

Figure 2. Optimized geometries of three conformers of $[HFIP{\cdot}X]^-$ (X = F, Cl, Br, and I) complex anions, calculated at the M06-2X level, where the distances of O−H and H···X bonds are noted with the unit of Å. The HFIP adopts the SP configuration in Iso A and AP in Iso B and C. ΔG values are relative Gibbs free energies (in eV) to the most stable structure.

new binding motif achieved via proton transfer from HFIP to F^- upon clustering in which the deprotonated HFIP anion interacts with a neutral HF molecule. As shown below, the abovementioned inferences on the complex structures and binding configurations are confirmed by using the quantum chemical calculations and bonding analyses.

3.2. Structures and Energetics of $[HFIP{\cdot}X]^-$ (X = F, Cl, Br, and I). DFT calculations were performed to identify the optimized structures of $[HFIP{\cdot}X]^-$ (X = F, Cl, Br, and I) complexes. Three conformers were taken into account for the complex structures, involving halide anions, that is, Iso A (HFIP in SP conformation with O−H···X^- interaction), Iso B (HFIP in AP conformation with O−H···X^- interaction), and Iso C (HFIP in AP conformation with C−H···X^- interaction).

Figure 2 shows the optimized geometries of $[HFIP{\cdot}X]^-$ (X = F, Cl, Br, and I) using the M06-2X functional and the corresponding relative Gibbs free energies to the most stable structure. For comparison, the optimized geometries of the neutral complexes and the isolated HFIP neutral were calculated at the same level too, as shown in Figures S1 and S2 of the Supporting Information. In fact, the structures in Figure 2 were confirmed to be the unique minima on potential energy surfaces for each halide anion along the O···H···X^- coordinate.

Apparently, the HFIP moiety in $[HFIP{\cdot}X]^-$ (X = Cl, Br, and I) almost remains its original structure of free HFIP neutral shown in Figure S2. Taking $[HFIP(SP){\cdot}Cl]^-$ (Iso A) for instance, the O−H bond length is slightly increased from 0.959 to 1.007 Å, and the distance between chloride and hydroxyl hydrogen atom is 1.951 Å. It is worth noting that this distance is apparently shorter than the typical HB length of the [O−H··· Cl] structure, indicative of formation of a stronger HB in the Cl^- case. Along the sequence of X^- = Cl^- → Br^- → I^-, the OH bond length in HFIP becomes shorter and the H···X^- distance increases (Figure 2), which is consistent with the halide PA trend.

In contrast to the other complex anions, $[HFIP{\cdot}F]^-$ shows a distinctively different binding motif in all three conformational isomers (Figure 2), that is, upon F^- and HFIP clustering, proton transfer occurs. In Iso A, the F···H distance is dramatically reduced to 1.048 Å, which is close to the covalent bond length of the HF molecule. Moreover, the O−H bond is elongated to 1.311 Å. Similar changes are also observed in Iso B and Iso C. Thus, the structure of $[HFIP_{-H}{\cdots}HF]^-$ is suggested in which the proton is shuffled from HFIP to fluoride. A similar phenomenon was reported in a recent study[47] on the $[HSO_4^-{\cdot}H^+{\cdot}F^-]$ complex, where the proton was found to transfer from H_2SO_4 to F^- to form $[HSO_4^-{\cdots}HF]$.

To identify the contributions of three conformers to the experimental spectra, their thermal populations are first estimated. As shown in Figure 2, Iso A is the most stable isomer among the three conformers, while Iso B has a higher energy ca. 0.3 eV for $[HFIP{\cdot}X]^-$ (X = Cl, Br, and I) and 0.10 eV for $[HFIP{\cdot}F]^-$, and Iso C lies >0.5 eV in energy above Iso A. These results differ from the $[HFIP{\cdot}H_2O]$ complex, where the SC and AP conformers of the HFIP moiety were confirmed with degenerate energies.[17] Considering the existence of additional orientation-specific charge−dipole interaction in the anionic $[HFIP{\cdot}X]^-$ clusters, it is conceivable that the SP structure of the HFIP moiety is favored and becomes the global minimum with appreciable energy differences from the AP conformation. More significantly, the $[HFIP{\cdot}X]^-$ complex

https://dx.doi.org/10.1021/acs.jpca.0c00024
J. Phys. Chem. A 2020, 124, 2036−2045

with an SC configurated HFIP moiety becomes unstable, as shown in Figure S3, despite the corresponding neutral HFIP being stable.

The contribution from Iso C can be safely neglected in the experiments because it has a relative energy > 0.5 eV above Iso A for X = F−I. Similarly, Iso B is not taken into account in the spectral analysis for $[HFIP{\cdot}X]^-$ (X = Cl, Br, and I) in which it lies ca. 0.3 eV higher in energy. However, as will be discussed below, the contribution of Iso B becomes evident in analyzing the $[HFIP{\cdot}F]^-$ spectrum, consistent with the fact that it is only slightly high in energy (0.10 eV).

Table 1 summarizes the calculated VDEs and ADEs using three different density functionals: B3LYP, ωB97XD, and M06-2X. In comparison with the experiments, the M06-2X values show the best agreement, for example, 4.18 (calc.) versus 4.15 eV (expt.) for the VDE and 4.03 (calc.) versus 4.03 eV (expt.) for the ADE of $[HFIP{\cdot}I]^-$, whereas both ωB97XD and B3LYP functionals overestimate the VDE and ADE of $[HFIP{\cdot}I]^-$. Consequently, only the relative energies at the M06-2X level are presented in the following discussions unless otherwise noted. The average deviations of the calculated and experimental VDEs and ADEs for $[HFIP{\cdot}X]^-$ (X = Cl, Br, I) are only 2.30 and 0.61%, respectively, lending appreciable credence for the optimized structures.

Figure 3 and Table S1 compare the calculated, experimental ΔEBEs, and calculated BEs for this series of complexes,

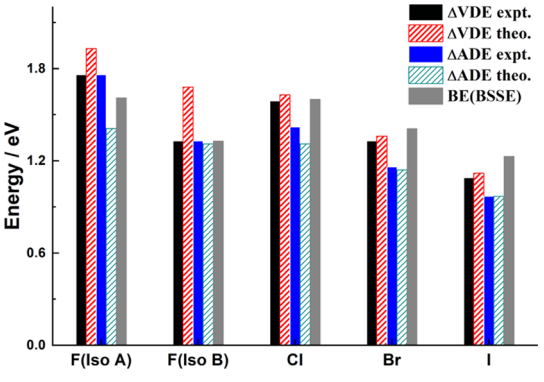

Figure 3. Comparison between the M06-2X calculated and experimental EBE shifts for $[HFIP{\cdot}X]^-$ complex anions relative to the corresponding isolated halide anions (X = Cl, Br, and I) and deprotonated HFIP anion (X = F). The calculated BEs between HFIP and X^- (X = Cl, Br, I) and between the deprotonated HFIP anion and HF are also shown.

exhibiting significant interactions between HFIP and halides that decrease along the halogen series for a given isomer (Iso A). The BEs of $[HFIP{\cdot}X]^-$ (X = Cl, Br, and I) are calculated as the interaction energy between HFIP and X^-, while for the X = F case, because the complex consists of $HFIP_{-H}^-$ anions and HF molecules, their BE should be calculated as the energy difference between the complex anion and the $HFIP_{-H}^-$ anion and neutral HF (eq 2). We will discuss it in Section 3.4.

3.3. Electron Density and Charge Population Analyses of $[HFIP{\cdot}X]^-$. Electron density, $\rho(r)$, and charge population analyses were carried out to help identify covalent versus HB properties for this series of complexes. Figure 4 shows the calculated renderings of the electron localization function[48] surface in the X−O−H plane using the optimized structures of $[HFIP{\cdot}X]^-$ (X = F, Cl, Br, and I). For $[HFIP{\cdot}X]^-$ (X = Cl, Br, and I), electron along the O−H−X path is

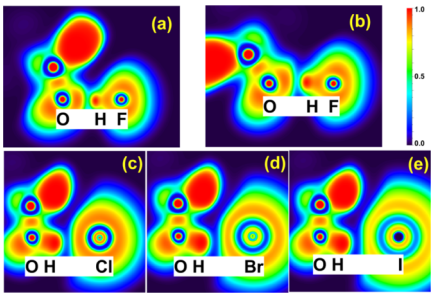

Figure 4. Electron density topological graphs of $[HFIP{\cdot}X]^-$ (X = F, Cl, Br, I) in the X−O−H plane: (a) $[HFIP{\cdot}F]^-$ in Iso A, (b) $[HFIP{\cdot}F]^-$ in Iso B, (c) $[HFIP{\cdot}Cl]^-$, (d) $[HFIP{\cdot}Br]^-$, and (e) $[HFIP{\cdot}I]^-$.

predominately localized between oxygen and hydrogen atoms, which is indicative of the covalent bonding of O−H. In contrast to the other complexes, $[HFIP{\cdot}F]^-$ in both Iso A and Iso B show entirely different electron density topological graphs (Figure 4a,b). A higher $\rho(r)$ between H−F than the O−H bond is clearly observed, which is further confirmed by the calculated potential energy density $V(r)$ (Table 2). The $V(r)$ value of the H−F bond equals to −0.4894 hartree and is nearly three times of that of the O−H bond (−0.1674 hartree), indicating that a covalent H−F bond is formed, accompanying with bond fission of the initial O−H bond in the HFIP moiety. The opposite results of $V(r)$ are found for the rest three complexes $[HFIP{\cdot}X]^-$ (X = Cl, Br, and I), as shown in Table 2. These conclusions agree with the related bond lengths as shown in their optimized geometries.

According to the "AIM" theory,[39,40] the topological property of electron density distribution depends on electron density $\rho(r)$ and the Laplacian quantity $\nabla^2\rho(r)$ of charge density. The bonding of two atoms may be classified into two groups: shared and closed-shell interactions, based on the distribution of $\rho(r)$ and the associated $\nabla^2\rho(r)$ at the bond critical point (BCP). The shared interaction has a large $\rho(r)$ and a negative $\nabla^2\rho(r)$ at the BCP, whereas a small $\rho(r)$ and a positive $\nabla^2\rho(r)$ exist for the closed-shell interaction. Thus, the topological properties of electron density at the BCPs (Figure S4 of the Supporting Information) for the complex anions are summarized in Table 2. The second derivatives of electron density in three-dimensional directions consisted of the Hessian matrix. Generally, when the three eigenvalues of the Hessian matrix are one positive and two negative, it is denoted as the key point of (3, −1), indicative of a chemical bond being formed between two atoms. Moreover, the more negative $\nabla^2\rho(r)$ implies the stronger covalent bond. In the $[HFIP{\cdot}X]^-$ (X = Cl, Br, and I) complex anions, all $\nabla^2\rho(r)$ values for the BCPs between oxygen and hydrogen atoms are negative and less than −2. Therefore, the covalent property of the O−H bond remains in these complex anions, and the Cl^-, Br^-, or I^- anions play the role of the charge inducer. However, in the $[HFIP{\cdot}F]^-$ anion, the $\nabla^2\rho(r)$ values of the O−H bond are significantly reduced to near zero, while that along with the H−F bond is changed to −1.1603 for Iso A and −1.5406 for Iso B. Thus, a strong covalent bond is reportedly formed between fluorine and hydrogen atoms, confirming the molecular structure of $[HFIP_{-H}^{-}\cdots HF]$.

NBO and MK analyses were further performed to identify charge distributions in the complex anions and neutrals. Table 3 summarizes the main calculated results. In $[HFIP{\cdot}X]^-$ (X = Cl, Br, and I), nearly 90% of the extra negative charge resides

https://dx.doi.org/10.1021/acs.jpca.0c00024
J. Phys. Chem. A 2020, 124, 2036−2045

Table 2. Topological Properties at the Critical Points in $[HFIP{\cdot}X]^-$ (X = F, Cl, Br, and I)

species	bond	$\rho(r)/(e{\cdot}Å^{-3})$	eigen of Hessian matrix λ_1	λ_2	λ_3	$\nabla^2\rho(r)$	$V(r)$/(hartree)
$[HFIP{\cdot}F]^-$ (Iso A)	F−H	0.2320	1.0483	−1.1046	−1.1040	−1.1603	−0.5045
	H−O	0.1227	0.7453	−0.3494	−0.3369	0.0589	−0.1644
$[HFIP{\cdot}F]^-$ (Iso B)	F−H	0.2584	1.2555	−1.3983	−1.3978	−1.5406	−0.5785
	H−O	0.0968	0.6167	−0.2413	−0.2333	0.1422	−0.1201
$[HFIP{\cdot}Cl]^-$	Cl−H	0.0457	−0.0644	0.1993	−0.0641	0.0708	−0.0381
	H−O	0.3062	−1.5565	0.9962	−1.5233	−2.0836	−0.6525
$[HFIP{\cdot}Br]^-$	Br−H	0.0334	−0.0391	0.1387	−0.0390	0.0606	−0.0229
	H−O	0.3208	−1.6531	1.0338	−1.6173	−2.2367	−0.6876
$[HFIP{\cdot}I]^-$	I−H	0.0252	0.0936	−0.0240	−0.0239	0.0457	−0.0141
	H−O	0.3298	1.0515	−1.7067	−1.6689	−2.3241	−0.7087

Table 3. NBO Analysis and MK (in Parentheses) Charge of Fragments for the Complex Anions $[HFIP{\cdot}X]^-$ and Neutrals [HFIP·X], Calculated with the Optimized Geometries of Anions

species	$[HFIP{\cdot}X]^-$ HFIP	X^-	[HFIP·X] HFIP	X
$[HFIP{\cdot}F]^-$ (Iso A)	−0.299 (−0.331)	−0.701 (−0.669)	+0.628 (+0.555)	−0.628 (−0.555)
$[HFIP{\cdot}F]^-$ (Iso B)	−0.320 (−0.374)	−0.680 (−0.626)	+0.540 (+0.367)	−0.540 (−0.367)
$[HFIP{\cdot}Cl]^-$	−0.125 (−0.165)	−0.875 (−0.835)	−0.072 (−0.082)	+0.072 (+0.082)
$[HFIP{\cdot}Br]^-$	−0.104 (−0.165)	−0.896 (−0.835)	−0.061 (−0.092)	+0.061 (+0.092)
$[HFIP{\cdot}I]^-$	−0.088 (−0.175)	−0.912 (−0.825)	−0.051 (−0.108)	+0.051 (+0.108)

on halogen anions as indicated by NBO analysis. The values on the fluorine atom of $[HFIP{\cdot}F]^-$ are reduced to −0.701 for Iso A and −0.680 for Iso B, which are close to the distribution of neutral HF molecules. Thus, the extra negative charge is transferred to the HFIP moiety during the intramolecular proton transfer process induced by the fluoride anion, indicating that the $HFIP_{-H}$ moiety is negatively charged in the complex anion indeed. Very similar results are obtained by the MK analysis of charge distributions. Therefore, these charge distribution analyses further confirm the expected structure of $[HFIP_{-H}{}^-{\cdot}HF]$ for the complex anion.

Moreover, Figure 5 shows the highest occupied molecular orbital (HOMO) of the closed shell complex anions. For $[HFIP{\cdot}X]^-$ (X = Cl, Br, and I), the HOMO is located on X^-,

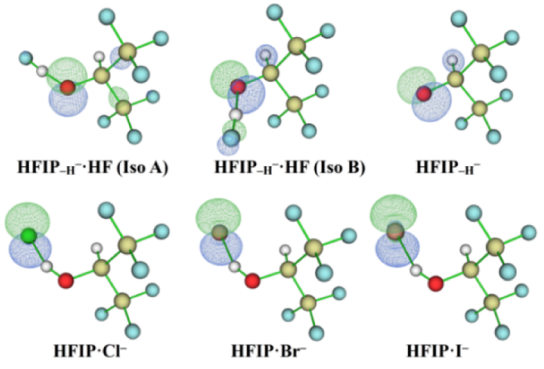

Figure 5. HOMO of the $[HFIP{\cdot}X]^-$ complex anions, as well as HOMO of the isolated $HFIP_{-H}{}^-$ anion, at their respective optimized geometries.

leading to its similar photodetachment spectral patterns when compared to the isolated X^-. However, based on the $[HFIP_{-H}{}^-{\cdots}HF]$ structure, the HOMO of $[HFIP{\cdots}F]^-$ mainly consists of the p orbital of negatively charged hydroxyl oxygen after losing a proton, regardless of Iso A and B. It is almost identical to the HOMO of the isolated $HFIP_{-H}{}^-$ anion, as shown in Figure 5. Therefore, the photodetached electron is validated from the HOMO of the $HFIP_{-H}{}^-$ moiety.

3.4. Assignments of Photodetachment Photoelectron Spectrum of $[HFIP{\cdot}F]^-$. Based on our theoretical calculations, the photoelectron spectrum, as shown in Figure 1a, should be contributed by the $[HFIP_{-H}{}^-{\cdots}HF]$ complex anion instead of $[HFIP{\cdots}F^-]$. Thus, the interaction between the negative charge group and neutral molecule, reflected by ΔADE or ΔVDE, should be referenced to the isolated deprotonated HFIP anion, that is, $HFIP_{-H}{}^-$. As shown in Table 1, ADE and VDE of the $[HFIP_{-H}{}^-{\cdots}HF]$ complex anion were calculated to be 4.91 and 5.50 eV for Iso A, 4.81 and 5.25 eV for Iso B, respectively. Based on the optimized geometries of the $HFIP_{-H}$ anion and its radical neutral (Figure S2), the ADE and VDE values of the $HFIP_{-H}{}^-$ anion were calculated to be 3.50 and 3.57 eV. Thus, ΔADE and ΔVDE are theoretically determined to be 1.41 and 1.93 eV for Iso A and 1.31 and 1.68 eV for Iso B, as shown in Figure 3. Moreover, the BE between the $HFIP_{-H}{}^-$ anion and HF molecule in the $[HFIP_{-H}{}^-{\cdots}HF]$ complex anion was calculated at the same level as BE = $E([HFIP_{-H}{}^-]) + E(HF) - E([HFIP_{-H}{}^-{\cdot}HF])$ with ZPE and BSSE corrections, for example, 1.61 eV for Iso A and 1.33 eV for Iso B. A smaller ΔEBE and BE for Iso B than Iso A originates because the charge−dipole interaction is orientation-specific. An estimation of charge−dipole interaction strength based on the point dipole approximation was performed and shown in Figure 6 to validate the conclusion. The calculation details, including dipole of the neutral moiety $\vec{\mu}$, orientation angle θ, and distance r between the charge and dipole, were described in Figure S5 of the Supporting Information.

For $[HFIP{\cdot}X^-]$ (X = Cl, Br, and I) in Iso A configuration, the estimated charge−dipole interaction strengths are 1.86, 1.69, and 1.47 eV, respectively. Compared with the calculated BE (BEES) values, as shown in Table S1, these values show a consistent trend along the atomic sequence of X^-, thus affirming the nature of the charge−dipole interaction. More significantly, the smaller dipole moment and the longer distance between the charge and the center of neutral HFIP in Iso B of $[HFIP{\cdot}X^-]$ are confirmed in comparison with Iso A. Hence, the charge−dipole interaction strengths in Iso B are much lower, for example, 0.38, 0.31, and 0.24 eV for the

https://dx.doi.org/10.1021/acs.jpca.0c00024
J. Phys. Chem. A 2020, 124, 2036−2045

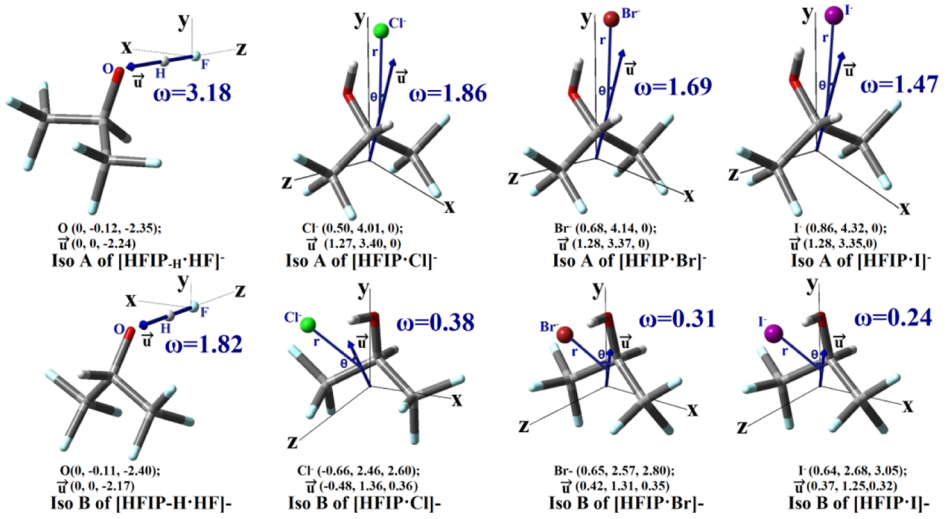

Figure 6. Charge−dipole interactions of the complex anions, $[HFIP_{-H}{\cdot}HF]^-$, $[HFIP{\cdot}Cl]^-$, $[HFIP{\cdot}Br]^-$, and $[HFIP{\cdot}I]^-$, with Iso A and Iso B configurations, where r is the distance of the charge from the center of the polar molecule, $\vec{\mu}$ is the dipole moment of the neutral polar molecule, θ is the angle between $\vec{r}$ and $\vec{\mu}$, and ω (in eV) represents the calculated interaction strengths.

complex anions (X^- = Cl^-, Br^-, and I^-), confirming the orientation-specific feature of the interaction.

The estimation in the case of $[HFIP{\cdot}F]^-$ is somewhat different because the charge population and the dipole are changed according to the $[HFIP_{-H}{}^-\cdots HF]$ structure. Based on the above NBO analysis, more than 90% negative charge is populated on the oxygen atom, and thus, the BE can be approximately calculated as the interaction between the point charge (O^-) and the neutral HF dipole. As shown in Figures 6 and S5, Iso A conformer of the $[HFIP{\cdot}F^-]$ complex anion is much more stable than Iso B, which is consistent with the abovementioned conclusions. However, these calculated values with the point dipole approximation have a moderate gap from the ab initio BEs, indicative of the more complicated forces in the complex besides the charge−dipole interaction.

To obtain the ΔADE or ΔVDE values of $[HFIP_{-H}{}^-{\cdot}HF]$ in experiments, an additional experiment was carried out to record the photoelectron spectrum of the isolated $HFIP_{-H}{}^-$ anion, under the identical experimental conditions, as shown in Figure 7a. The Franck−Condon simulated spectrum is generally consistent with the experimental result, except for the weaker intensity in high-energy side. As suggested by the simulation, the resolved vibrational structure was dominated by the excitation of the O−C−H bending vibration mode. The ADE and VDE of $HFIP_{-H}{}^-$ anions were experimentally determined to be 3.43 and 3.75 eV, respectively.

To facilitate the comparison, the NIPE spectrum of the $[HFIP_{-H}{}^-{\cdot}HF]$ complex anion is shown again in Figure 7b. The spectrum of the $[HFIP_{-H}{}^-{\cdot}HF]$ complex is significantly broader than that of $HFIP_{-H}{}^-$, with discernible fine structures at low-energy side similar to the $HFIP_{-H}{}^-$ anion. The considerable breadth of the complex spectrum implies that there may be more than one isomer contributing to the spectrum. Iso A of $[HFIP_{-H}{}^-{\cdot}HF]$ is calculated to be only 0.10 eV more stable than Iso B, and the calculated ADE of Iso A is 0.4 eV higher than Iso B. Thus, a viable explanation that accounts for the spectral breadth is to consider both Iso A and Iso B. However, as indicated in the experimental and simulated spectra (Figure 7a), it will be extremely challenging if not impossible to directly perform the Franck−Condon simulation of the complex anion to obtain the contributions of each

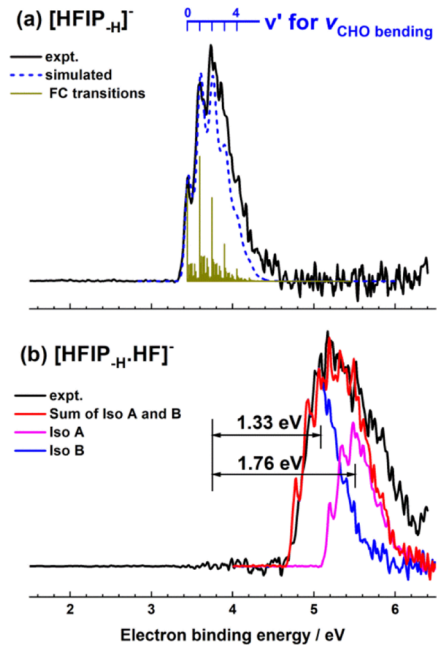

Figure 7. Low-temperature photoelectron spectra of the isolated $HFIP_{-H}{}^-$ anion (a) and the $[HFIP_{-H}{}^-{\cdot}HF]$ complex anion (b) at 193 nm. For the isolated $HFIP_{-H}{}^-$ anion, the Franck−Condon transitions and the simulated spectrum with fwhm of 80 meV are shown as well in which the observed vibrational structure is assigned to the excitation of O−C−H bending vibration. For the complex anion, the simulated spectrum (red) is the sum of two spectra of two conformers (Iso A and B), plotted by blue and purple lines, respectively.

conformer because only qualitative agreement has been achieved between the simulation and experiment at the high-energy tail for the isolated $HFIP_{-H}{}^-$ anion. Consequently, an alternative and simple strategy was used to fit the spectrum of the complex anion. As the optimized geometries of the $HFIP_{-H}$ moiety in the isolated $HFIP_{-H}{}^-$ and $[HFIP_{-H}{}^-{\cdot}HF]$ complex anion (Iso A and B) are nearly identical, it is natural to conceive that the PE spectrum of each conformer has the same pattern as the isolated $HFIP_{-H}{}^-$ anion because of its role of an electron emitter. Thus, the observed complex spectrum

https://dx.doi.org/10.1021/acs.jpca.0c00024
J. Phys. Chem. A 2020, 124, 2036−2045

can be roughly simulated with a double-peak scheme (see Figure 7b), where the different ΔEBEs for the two conformers were considered because of the different interactions between $HFIP_{-H^-}$ anions and HF molecules in Iso A and Iso B. Moreover, the intensities of two peaks are the product of electron photodetachment cross section and thermal populations of the isomers. Therefore, based on the expected smaller population of Iso B than Iso A, the photodetachment cross section of Iso B should be much higher than Iso A, which is consistent with the weaker interaction between $HFIP_{-H^-}$ and HF moieties in Iso B.

Based on the abovementioned spectral assignments, the experimental ΔEBE values were determined, for example, 1.76 eV for Iso A and 1.33 eV for Iso B. A general consistency between the theory and experiment is obtained, as shown in Figure 3. Because the spectral profiles of two conformers are assumed to be identical to that of the isolated $HFIP_{-H^-}$, ΔADE and ΔVDE must have the same values for each isomer, and therefore, the moderate deviations from the experimental data are acceptable considering such a crude approximation in spectral simulation.

4. CONCLUSIONS

We reported a joint experimental and theoretical study on the intermolecular interactions between HFIP and halide anions X^- = F^-, Cl^-, Br^-, and I^-. For $[HFIP{\cdot}X]^-$ (X = Cl, Br, and I), the resultant photoelectron spectra maintain the corresponding halide spectral characters with only blueshifts in EBE, suggesting the halide anion as a electron emission chromophore. Quantum chemical calculations, including geometry optimization, electron density, and charge distribution analyses, all indicate that these three complexes are formed with the $[HFIP{\cdots}X^-]$ structure in which X^- interacts with the neutral HFIP via ionic hydrogen bonding and charge−dipole interactions. The much stronger $HFIP{\cdots}X^-$ interactions in the anionic state than that of $HFIP{\cdots}X^{\bullet}$ in the neutral complexes give rise to the significant EBE blueshifts. The HFIP adopts SP configuration upon interacting with halides, determined by the strong charge−dipole interactions that prefer the SP structure for HFIP.

In contrast to the X = Cl, Br, and I cases, the spectrum of $[HFIP{\cdot}F]^-$ completely differs from that of F^- but similar to that of the isolated $HFIP_{-H^-}$ anion, albeit with a much broadened spectral width. The theoretical calculations validate the formation of the stable structure of $[HFIP_{-H^-}{\cdots}HF]$ in which the proton is transferred from the HFIP moiety to F^- driven by the much strong PA of F^-. Two conformers, Iso A and Iso B with the $HFIP_{-H}$ moiety in the SP and AP configuration, respectively, are found to lie close in energy. The experimental spectrum can be simulated by considering contributions from both isomers. The obtained much smaller ΔEBE and BE for Iso B than Iso A clearly demonstrate that the charge−dipole interaction is orientation-specific indeed.

■ ASSOCIATED CONTENT

Supporting Information

The Supporting Information is available free of charge at https://pubs.acs.org/doi/10.1021/acs.jpca.0c00024.

Optimized structures of neutral HFIP·X (X = F, Cl, Br, and I) complexes and $HFIP_{-H}$ radical anion and neutral; relaxed potential energy surface of the OH torsion (dihedral angle H1−C−O−H2) for neutral HFIP and $[HFIP{\cdot}F]^-$ complex anions; bond critical points and ΔEBEs of the stable complex anions; and charge−dipole interactions of $[HFIP{\cdot}X^-]$ (X = F, Cl, Br, and I) (PDF)

■ AUTHOR INFORMATION

Corresponding Authors

Xiaoguo Zhou − *Hefei National Laboratory for Physical Sciences at the Microscale, Department of Chemical Physics, University of Science and Technology of China, Hefei, Anhui 230026, P. R. China;* orcid.org/0000-0002-0264-0146; Email: xzhou@ustc.edu.cn

Xue-Bin Wang − *Physical Sciences Division, Pacific Northwest National Laboratory, Richland, Washington 99352, United States;* orcid.org/0000-0001-8326-1780; Email: xuebin.wang@pnnl.gov

Authors

Lei Wang − *Hefei National Laboratory for Physical Sciences at the Microscale, Department of Chemical Physics, University of Science and Technology of China, Hefei, Anhui 230026, P. R. China*

Qinqin Yuan − *Physical Sciences Division, Pacific Northwest National Laboratory, Richland, Washington 99352, United States*

Wenjin Cao − *Physical Sciences Division, Pacific Northwest National Laboratory, Richland, Washington 99352, United States;* orcid.org/0000-0002-2852-4047

Jia Han − *Hefei National Laboratory for Physical Sciences at the Microscale, Department of Chemical Physics, University of Science and Technology of China, Hefei, Anhui 230026, P. R. China*

Shilin Liu − *Hefei National Laboratory for Physical Sciences at the Microscale, Department of Chemical Physics, University of Science and Technology of China, Hefei, Anhui 230026, P. R. China*

Complete contact information is available at: https://pubs.acs.org/10.1021/acs.jpca.0c00024

Notes

The authors declare no competing financial interest.

■ ACKNOWLEDGMENTS

This work was supported by U.S. Department of Energy (DOE), Office of Science, Office of Basic Energy Sciences, Division of Chemical Sciences, Geosciences, and Biosciences, and performed using EMSL, a national scientific user facility sponsored by DOE's Office of Biological and Environmental Research and located at Pacific Northwest National Laboratory, which is operated by Battelle Memorial Institute for the DOE. Financial support of the National Natural Science Foundation of China (nos. 21573210 and 21873089), the National Key Research and Development Program of China (no. 2016YFF0200502), and the Ministry of Science and Technology of China (no. 2012YQ220113) are also gratefully acknowledged.

■ REFERENCES

(1) Colomer, I.; Chamberlain, A. E. R.; Haughey, M. B.; Donohoe, T. J. Hexafluoroisopropanol as a highly versatile solvent. *Nat. Rev. Chem.* **2017**, *1*, 0088.

(2) Miura, Y.; Satoh, T.; Narumi, A.; Nishizawa, O.; Okamoto, Y.; Kakuchi, T. Synthesis of well-defined syndiotactic poly(methyl methacrylate) with low-temperature atom transfer radical polymer-

ization in fluoroalcohol. *J. Polym. Sci., Part A: Polym. Chem.* **2006**, *44*, 1436−1446.
(3) Wang, W.; Zhang, Z.; Zhu, J.; Zhou, N.; Zhu, X. Single electron transfer-living radical polymerization of methyl methacrylate in fluoroalcohol: Dual control over molecular weight and tacticity. *J. Polym. Sci., Part A: Polym. Chem.* **2009**, *47*, 6316−6327.
(4) Wang, W.; Zhao, J.; Yu, H.; Zhou, N.; Zhang, Z.; Zhu, X. Simultaneously improving controls over molecular weight and stereoregularity of Poly(4-vinylpyridine) via a hydrogen bonding-facilitated controlled radical polymerization. *Polymer* **2013**, *54*, 3248−3253.
(5) Liu, Q.; Wu, H.; Zhang, L.; Zhou, Y.; Zhang, W.; Pan, X.; Zhang, Z.; Zhu, X. RAFT polymerization of N-vinylpyrrolidone mediated by cyanoprop-2-yl-1-dithionaphthalate in the presence of a fluoroalcohol: The possibility of altering monomer properties by hydrogen bonding? *Polym. Chem.* **2016**, *7*, 2015−2021.
(6) Wu, H.; Wan, Y.; Wang, W.; Wang, Y.; Zhou, N.; Zhang, W.; Li, X.; Zhang, Z.; Zhu, X. Hydrogen bonding promoting the controlled radical polymerization of 2-vinyl pyridine: supramonomer for better control. *Polym. Chem.* **2015**, *6*, 2620−2625.
(7) Gieshoff, T.; Schollmeyer, D.; Waldvogel, S. R. Access to pyrazolidin-3, 5-diones through anodic N−N bond formation. *Angew. Chem., Int. Ed.* **2016**, *55*, 9437−9440.
(8) Kirste, A.; Nieger, M.; Malkowsky, I. M.; Stecker, F.; Fischer, A.; Waldvogel, S. R. Ortho-selective phenol-coupling reaction by anodic treatment on boron-doped diamond electrode using fluorinated alcohols. *Chem.—Eur. J.* **2009**, *15*, 2273−2277.
(9) Herrmann, I. K.; Castellon, M.; Schwartz, D. E.; Hasler, M.; Urner, M.; Hu, G.; Minshall, R. D.; Beck-Schimmer, B. Intravenous application of a primary sevoflurane metabolite improves outcome in murine septic peritonitis: First results. *PLoS One* **2013**, *8*, No. e72057.
(10) Myhre, G.; Shindell, D.; Bréon, F. M.; Collins, W.; Fuglestvedt, J.; Huang, J.; Koch, D.; Lamarque, J. F.; Lee, D.; Mendoza, B.; et al. Anthropogenic and Natural Radiative Forcing. In *Climate Change 2013: The Physical Science Basis. Contribution of Working Group I to the Fifth Assessment Report of the Intergovernmental Panel on Climate Change*; Stocker, T. F., Qin, D., Plattner, G. K., Tignor, M. S., Allen, K., Boschung, J., Nauels, A., Xia, Y., Bex, V., Midgley, P. M., Eds.; Cambridge University Press; Cambridge, United Kingdom and New York, NY, USA, 2013.
(11) Godin, P. J.; Le Bris, K.; Strong, K. Conformational analysis and global warming potentials of 1,1,1,3,3,3-hexafluoro-2-propanol from absorption spectroscopy. *J. Quant. Spectrosc. Radiat. Transfer* **2017**, *203*, 522−529.
(12) Berrien, J.-F.; Ourévitch, M.; Morgant, G.; Ghermani, N. E.; Crousse, B.; Bonnet-Delpon, D. A crystalline H-bond cluster of hexafluoroisopropanol (HFIP) and piperidine. *J. Fluorine Chem.* **2007**, *128*, 839−843.
(13) Shahi, A.; Arunan, E. Microwave spectrum of hexafluoroisopropanol and torsional behavior of molecules with a CF_3-C-CF_3 group. *J. Phys. Chem. A* **2015**, *119*, 5650−5657.
(14) Czarnik-Matusewicz, B.; Pilorz, S.; Bieńko, D.; Michalska, D. Molecular and electronic structures, infrared spectra, and vibrational assignment for ap and sc conformers of hexafluoro-iso-propanol. *Vib. Spectrosc.* **2008**, *47*, 44−52.
(15) Durig, J. R.; Larsen, R. A.; Cox, F. O.; Van der Veken, B. J. Raman and far-infrared spectra of gaseous 1,1,1,3,3,3-hexafluoro-2-propanol, conformational stability and barriers to internal rotation. *J. Mol. Struct.* **1988**, *172*, 183−201.
(16) Fioroni, M.; Burger, K.; Mark, A. E.; Roccatano, D. Model of 1,1,1,3,3,3-Hexafluoro-propan-2-ol for Molecular Dynamics Simulations. *J. Phys. Chem. B* **2001**, *105*, 10967−10975.
(17) Shahi, A.; Arunan, E. Microwave spectroscopic and theoretical investigations of the strongly hydrogen bonded hexafluoroisopropanol···water complex. *Phys. Chem. Chem. Phys.* **2015**, *17*, 24774−24782.
(18) Yoshida, K.; Yamaguchi, T.; Adachi, T.; Otomo, T.; Matsuo, D.; Takamuku, T.; Nishi, N. Structure and dynamics of hexafluoroisopropanol-water mixtures by x-ray diffraction, small-angle neutron scattering, NMR spectroscopy, and mass spectrometry. *J. Chem. Phys.* **2003**, *119*, 6132−6142.
(19) Hollóczki, O.; Berkessel, A.; Mars, J.; Mezger, M.; Wiebe, A.; Waldvogel, S. R.; Kirchner, B. The catalytic effect of fluoroalcohol mixtures depends on domain formation. *ACS Catal.* **2017**, *7*, 1846−1852.
(20) Leboeuf, D.; Marin, L.; Michelet, B.; Perez-Luna, A.; Guillot, R.; Schulz, E.; Gandon, V. Harnessing the lewis acidity of hFIP through its cooperation with a Calcium(II) salt: Application to the aza-piancatelli reaction. *Chem.—Eur. J.* **2016**, *22*, 16165−16171.
(21) Qi, C.; Gandon, V.; Lebœuf, D. Calcium(II)-catalyzed intermolecular hydroarylation of deactivated styrenes in hexafluoroisopropanol. *Angew. Chem., Int. Ed.* **2018**, *57*, 14245−14249.
(22) Hankache, J.; Hanss, D.; Wenger, O. S. Hydrogen-bond strengthening upon photoinduced electron transfer in ruthenium-anthraquinone dyads interacting with hexafluoroisopropanol or water. *J. Phys. Chem. A* **2012**, *116*, 3347−3358.
(23) Simpson, W. R.; Brown, S. S.; Saiz-Lopez, A.; Thornton, J. A.; von Glasow, R. Tropospheric halogen chemistry: Sources, cycling, and impacts. *Chem. Rev.* **2015**, *115*, 4035−4062.
(24) Ariya, P. A.; Khalizov, A.; Gidas, A. Reactions of gaseous mercury with atomic and molecular halogens: Kinetics, product studies, and atmospheric implications. *J. Phys. Chem. A* **2002**, *106*, 7310−7320.
(25) Hou, G.-L.; Zhang, J.; Valiev, M.; Wang, X.-B. Structures and energetics of hydrated deprotonated cis-pinonic acid anion clusters and their atmospheric relevance. *Phys. Chem. Chem. Phys.* **2017**, *19*, 10676−10684.
(26) Yuan, Q.; Kong, X.-T.; Hou, G.-L.; Jiang, L.; Wang, X.-B. Electrospray ionization photoelectron spectroscopy of cryogenic $[EDTA{\cdot}\,M\,(ii)]^{2-}$ complexes (M= Ca, V−Zn): Electronic structures and intrinsic redox properties. *Faraday Discuss.* **2019**, *217*, 383−395.
(27) Hou, G.-L.; Lin, W.; Deng, S. H. M.; Zhang, J.; Zheng, W.-J.; Paesani, F.; Wang, X.-B. Negative ion photoelectron spectroscopy reveals thermodynamic advantage of organic acids in facilitating formation of bisulfate ion clusters: Atmospheric implications. *J. Phys. Chem. Lett.* **2013**, *4*, 779−785.
(28) Zhang, J.; Zhou, B.; Sun, Z.-R.; Wang, X.-B. Photoelectron spectroscopy and theoretical studies of anion-π interactions: binding strength and anion specificity. *Phys. Chem. Chem. Phys.* **2015**, *17*, 3131−3141.
(29) Wang, X.-B.; Wang, L.-S. Development of a low-temperature photoelectron spectroscopy instrument using an electrospray ion source and a cryogenically controlled ion trap. *Rev. Sci. Instrum.* **2008**, *79*, 073108.
(30) Wang, X.-B. Cluster model studies of anion and molecular specificities via electrospray ionization photoelectron spectroscopy. *J. Phys. Chem. A* **2017**, *121*, 1389−1401.
(31) Krishnan, R.; Binkley, J. S.; Seeger, R.; Pople, J. A. Self-consistent molecular orbital methods. XX. A basis set for correlated wave functions. *J. Chem. Phys.* **1980**, *72*, 650−654.
(32) Peterson, K. A.; Figgen, D.; Goll, E.; Stoll, H.; Dolg, M. Systematically convergent basis sets with relativistic pseudopotentials. II. Small-core pseudopotentials and correlation consistent basis sets for the post-d group 16-18 elements. *J. Chem. Phys.* **2003**, *119*, 11113.
(33) Schuchardt, K. L.; Didier, B. T.; Elsethagen, T.; Sun, L.; Gurumoorthi, V.; Chase, J.; Li, J.; Windus, T. L. Basis set exchange: A community database for computational sciences. *J. Chem. Inf. Model.* **2007**, *47*, 1045−1052.
(34) Liu, B.; McLean, A. D. Accurate calculation of the attractive interaction of two ground state helium atoms. *J. Chem. Phys.* **1973**, *59*, 4557−4558.
(35) Boys, S. F.; Bernardi, F. The calculation of small molecular interactions by the differences of separate total energies. Some procedures with reduced errors. *Mol. Phys.* **1970**, *19*, 553−566.
(36) Reed, A. E.; Curtiss, L. A.; Weinhold, F. Intermolecular interactions from a natural bond orbital, donor-acceptor viewpoint. *Chem. Rev.* **1988**, *88*, 899−926.

https://dx.doi.org/10.1021/acs.jpca.0c00024
J. Phys. Chem. A 2020, 124, 2036−2045

(37) Singh, U. C.; Kollman, P. A. An approach to computing electrostatic charges for molecules. *J. Comput. Chem.* **1984**, *5*, 129−145.
(38) Frisch, M. J.; Trucks, G. W.; Schlegel, H. B.; Scuseria, G. E.; Robb, M. A.; Cheeseman, J. R.; Scalmani, G.; Barone, V.; Mennucci, B.; Petersson, G. A.; et al. *Gaussian 09*, Revision E.01; Gaussian, Inc.: Wallingford CT, 2009.
(39) Bader, R. F. W. Comment on the comparative use of the electron density and its Laplacian. *Chem.—Eur. J.* **2006**, *12*, 7769−7772.
(40) Bader, R. F. W.; Essén, H. The characterization of atomic interactions. *J. Chem. Phys.* **1984**, *80*, 1943−1960.
(41) Lu, T.; Chen, F. Multiwfn: A multifunctional wavefunction analyzer. *J. Comput. Chem.* **2012**, *33*, 580−592.
(42) Mozhayskiy, V. A.; Krylov, A. I. *ezSpectrum*, version 3.0; University of Southern California: Los Angeles, CA, 2016, http://iopenshell.usc.edu/downloads.
(43) Arnold, D. W.; Bradforth, S. E.; Kim, E. H.; Neumark, D. M. Study of halogen−carbon dioxide clusters and the fluoroformyloxyl radical by photodetachment of $X^-(CO_2)$(X= I, Cl, Br) and FCO^-_2. *J. Chem. Phys.* **1995**, *102*, 3493−3509.
(44) Cheng, M.; Feng, Y.; Du, Y.; Zhu, Q.; Zheng, W.; Czakó, G.; Bowman, J. M. Communication: Probing the entrance channels of the X + CH_4 → HX + CH_3 (X= F, Cl, Br, I) reactions via photodetachment of X^-−CH_4. *J. Chem. Phys.* **2011**, *134*, 191102.
(45) Swart, M.; Bickelhaupt, F. M. Proton affinities of anionic bases: trends across the periodic table, structural effects, and DFT validation. *J. Chem. Theory Comput.* **2006**, *2*, 281−287.
(46) Taft, R. W.; Koppel, I. A.; Topsom, R. D.; Anvia, F. Acidities of OH compounds, including alcohols, phenol, carboxylic acids, and mineral acids. *J. Am. Chem. Soc.* **1990**, *112*, 2047−2052.
(47) Hou, G.-L.; Wang, X.-B. Spectroscopic signature of proton location in proton bound $HSO4^-$• H^+• X^-(X= F, Cl, Br, and I) clusters. *J. Phys. Chem. Lett.* **2019**, *10*, 6714−6719.
(48) Silvi, B.; Savin, A. Classification of chemical bonds based on topological analysis of electron localization functions. *Nature* **1994**, *371*, 683−686.

https://dx.doi.org/10.1021/acs.jpca.0c00024
J. Phys. Chem. A 2020, 124, 2036−2045